

Fidelity-Age–Aware Scheduling in Quantum Repeater Networks

Ozgur Ercetin, Zafer Gedik

Faculty of Engineering and Natural Sciences,

Sabanci University, Istanbul, TR.

Abstract

Quantum repeater networks distribute entanglement over long distances but must balance fidelity, delay, and resource contention. Prior work optimized throughput and end-to-end fidelity, yet little attention has been paid to the freshness of entanglement—the time since a usable Bell pair was last delivered. We introduce the Fidelity-Age (FA) metric, which measures this interval for states whose fidelity exceeds a threshold F_{\min} . A renewal formulation links slot-level success probability to long-run average FA, enabling a stochastic control problem that minimizes FA under budget and memory limits. Two lightweight schedulers, FA-THR and FA-INDEX, approximate Lyapunov-drift-optimal control. Simulations on slotted repeater grids show that FA-aware scheduling preserves throughput while reducing extreme-age events by up to two orders of magnitude. Fidelity-Age thus provides a tractable, physically grounded metric for reliable and timely entanglement delivery in quantum networks.

I. Introduction

Quantum repeater networks extend point-to-point quantum key distribution (QKD) links toward multi-hop entanglement distribution across large-scale topologies [1], [2]. Their applications—ranging from distributed quantum computation to high-rate secret key generation—depend on the timely delivery of entangled Bell pairs whose fidelities exceed a task-specific threshold.

Unlike classical packets, entangled states are transient physical resources. Their fidelity decays with storage time due to decoherence, and both entanglement swapping and purification introduce random delays and success probabilities [3], [4]. As a result, the usefulness of an entanglement link depends not only on how often it is established but also on when

it was last refreshed. Delivering a pair that has decohered below a minimum fidelity F_{\min} is equivalent to a delivery failure.

Existing work optimizes throughput and end-to-end fidelity in repeater networks [5]–[9], yet there is little theory on quantifying or controlling the freshness of distributed entanglement. In classical communication systems, the Age of Information (AoI) formalism provides a stochastic measure of update timeliness and has yielded provably optimal scheduling rules [10], [11]. An analogous metric for quantum networks has been missing.

This paper introduces the Fidelity-Age (FA) metric, which measures the time elapsed since the most recent delivery of an entangled pair with fidelity at least F_{\min} . FA couples temporal freshness with physical-layer quality and directly reflects decoherence, probabilistic link generation, purification outcomes, and swapping success.

The main contributions are:

- We define the FA process and derive its renewal identity, establishing a direct relation between slot-level usable-delivery probability and long-run expected FA.
- We formulate a stochastic control problem minimizing average FA under attempt-budget and memory constraints.
- We propose practical FA-aware scheduling policies—FA-THR and FA-INDEX—motivated by Lyapunov-drift minimization, and evaluate their performance under finite-coherence and heterogeneous-path conditions.

By linking physical fidelity evolution to a renewal-based freshness metric, this work provides a quantitative foundation for age-aware control in quantum repeater networks. It shows that explicit fidelity-age weighting yields schedules that are simultaneously efficient, fair, and stable under realistic decoherence limits.

II. Background and Related Work

A. Qubits, Bell States, and Fidelity

A qubit is a unit vector in \mathbb{C}^2 , $|\psi\rangle = \alpha|0\rangle + \beta|1\rangle$ with $|\alpha|^2 + |\beta|^2 = 1$. Two-qubit Bell states serve as maximally entangled targets; for example $|\Phi^+\rangle = (|00\rangle + |11\rangle)/\sqrt{2}$.

Quantum memories store entangled states temporarily until successful swapping or purification can be performed. However, stored states decohere exponentially with time, reducing their fidelity. For a produced two-qubit state with density matrix ρ , the (state) fidelity with

respect to a target pure state $|\psi_{\text{tar}}\rangle$ is

$$F = \langle \psi_{\text{tar}} | \rho | \psi_{\text{tar}} \rangle. \quad (1)$$

We adopt the common Werner approximation for noisy pairs: write $p_W = (4F - 1)/3 \in [0, 1]$. Storage for one slot maps $p_W \mapsto p_W e^{-\Delta/T_2}$, equivalently

$$F(\tau + 1) = 1 - (1 - F(\tau))e^{-\Delta/T_2}, \quad (2)$$

and end-to-end Werner composition across a k -edge path yields $p_{W,\text{end}} = \prod_{j=1}^k p_{W,e_j}$ and

$$F_{\text{end}} = \frac{1 + 3p_{W,\text{end}}}{4}. \quad (3)$$

When $F(\tau)$ (F_{end}) drops below a task-specific minimum threshold F_{\min} , the state becomes unusable and must be discarded.

B. Freshness and the Fidelity-Age Metric

In classical networking, the Age of Information (AoI) framework quantifies the timeliness of received updates by measuring the time elapsed since the most recent successful delivery. Inspired by this concept, we define the Fidelity-Age (FA) metric as the time since the last delivery of an entangled pair whose fidelity exceeds F_{\min} . The FA process thus couples temporal freshness with physical-layer quality, reflecting both stochastic link success and fidelity evolution due to decoherence. Minimizing long-run average FA corresponds to maintaining high-quality entanglement with minimal delay between usable deliveries.

C. Related Work

Prior work on quantum repeater networks can be grouped into three themes—(i) multi-hop architectures and routing, (ii) fidelity management via purification and memory constraints, and (iii) network-level scheduling and resource allocation. We position the proposed Fidelity-Age (FA) metric at the intersection of (ii)–(iii) by providing a freshness-oriented objective that explicitly couples stochastic delivery, fidelity thresholds, and decoherence.

Early work established routing and multi-hop entanglement distribution models under realistic repeater operations [5]. More recent surveys clarify the physical trade-offs that link achievable rate, distance, and fidelity [12]. Building on these foundations, router-style multiplexing and end-to-end path optimization with explicit fidelity targets and memory awareness have been formulated via ILPs and scalable heuristics [13], [14]. Related protocol lines, including distance-independent-rate and packet-switching approaches, further motivate control at the network layer beyond single repeater chains [15], [16].

A key determinant of end-to-end usability is purification: both where purification is performed and how many rounds are scheduled. Recent results show that network-level scheduling of purification can substantially outperform fixed-depth designs [17]. Separately, finite-memory and finite-coherence studies quantify rate losses due to limited storage time and highlight the need for policies that account for decoherence-induced fidelity decay [18]. Work on reusing pre-existing entanglements likewise emphasizes that temporal state (what is already stored, and how old it is) can change path-selection decisions and reduce latency [19].

At the control layer, scheduling decisions are computationally difficult (often NP-hard) and have been studied using exact formulations, heuristics, and reinforcement learning, with objectives such as throughput, fairness across requests, or utility maximization [20]–[22]. These efforts typically assume a notion of success/utility per slot, but they do not provide a unified freshness metric that directly measures the cost of delayed usable deliveries under fidelity decay.

While quantum networking lacks a standardized “age” metric for entanglement, the classical Age-of-Information (AoI) literature offers a principled framework for freshness-aware optimization, including Lyapunov-drift methods [11]. We adapt this viewpoint to repeater networks by defining Fidelity-Age (FA): successful deliveries with end-to-end fidelity at least F_{\min} serve as renewal events, and the time since the most recent such delivery quantifies freshness-conditioned usability. Relative to routing and path-optimization work [5], [13], [14], purification scheduling [17], and general scheduling approaches [19]–[22], our focus is an objective and analysis framework that integrates (a) stochastic entanglement generation and swapping, (b) fidelity thresholds, and (c) decoherence over finite coherence times, yielding scheduling rules explicitly targeted at freshness-conditioned usability.

III. System Model

We formalize a slotted quantum-repeater network on an explicit probability space and specify storage, decoherence, purification, and swapping so that the model is consistent with the numerical experiments.

A. Network Architecture

A software-defined network (SDN) controller maintains a global view of link states and stored pairs, issues per-slot commands for link attempts, swapping, and optional purification,

and uses the classical control plane to coordinate quantum operations. Each intermediate repeater holds two quantum memories to serve its two incident links in a line topology; end nodes hold one memory per active end-to-end demand. When entanglement diversity (parallel path attempts or later distillation) is enabled, end nodes allocate an extra memory unit per additional concurrent end-to-end (e2e) attempt. A path is a simple sequence of physical links connecting a source–destination pair. The controller may reuse prior entanglements left from previous cycles on any subset of path edges. Reuse can tilt decisions toward longer paths that already hold stored pairs. Unless stated otherwise, hardware is uniform: equal inter-nodal distances, identical sources and BSM modules.

B. Probabilistic Slotted Graph Model

Let $G = (V, E)$ be a connected undirected graph of repeaters and lossy optical links. Time is slotted with fixed slot duration $\Delta > 0$; slots are indexed by $t \in \mathbb{N}$. The system is defined on $(\Omega, \mathcal{F}, \mathbb{P})$.

Each edge $e \in E$ has $S(e) \in \mathbb{N}$ parallel modes. In slot t , mode $i \in \{1, \dots, S(e)\}$ attempts a link-level entanglement with success indicator

$$X_t^{(i)}(e) \sim \text{Bernoulli}(p_0(e)),$$

$$p_0(e) = \eta(e), \quad \eta(e) = \exp(-\alpha L(e)),$$

where $L(e)$ is the link length and $\alpha > 0$ is the fiber loss coefficient (km^{-1}) [23].

Remark 1 (Independence). The random variables $\{X_t^{(i)}(e)\}$ are independent across e , i , and t , and independent of all Bell-state measurement (BSM) and purification outcomes.

The number of successful link-level pairs on e in slot t is

$$N_t(e) = \sum_{i=1}^{S(e)} X_t^{(i)}(e) \sim \text{Binomial}(S(e), p_0(e)).$$

The per-edge success probability (at least one success on e) is

$$p_{\text{link}}(e) = 1 - (1 - p_0(e))^{S(e)}.$$

We cap the number of retained pairs per edge per slot by $m_{\max}(e) \in \mathbb{N}$:

$$N_t^{\text{ret}}(e) = \min\{N_t(e), m_{\max}(e)\}.$$

Note that $m_{\max}(e) = 1$ when there is no purification, whereas $m_{\max}(e) \geq 2$ when there is.

We also define the external multigraph $\mathcal{H}_t^{\text{multi}}$ whose edge multiplicity on e equals $N_t^{\text{ret}}(e)$, and its simple support

$$\mathcal{H}_t = \{e \in E : N_t^{\text{ret}}(e) \geq 1\}.$$

C. Internal phase: purification and swapping

Internal operations are local to repeaters and occur after the external phase within the same slot. We adopt the standard BBPSSW entanglement purification protocol with a fixed noise model (bit-flip or Werner) throughout the experiments; see [24] for the explicit maps and success probabilities. In all cases, input-pair fidelities already include storage decay via (2).

We assume independent BSMs at intermediate repeaters with per-repeater success probability $q \in (0, 1]$. For a path with k edges, a swap attempt succeeds with probability q^{k-1} , conditional on one available pair per edge and independence across repeaters [23].

Edge pairs are modeled as Werner states. Conditioned on successful swaps, the end-to-end state remains Werner with a parameter equal to the product of edge parameters; we use this only to check usability $F_{\text{end}}(\pi) \geq F_{\min}$ and omit the standard closed forms [23]. For $T_{\text{mem}} > 1$, edge fidelities already include storage decay and any in-slot purification.

D. Usable deliveries and success events

Fix a set \mathcal{P} of source–destination requests. An application-level threshold $F_{\min} \in (1/4, 1)$ defines usable deliveries. In slot t , for flow (s, d) we say a usable delivery occurs if there exists a simple path $\pi \subseteq \mathcal{H}_t$ from s to d with $k := |\pi|$ edges such that:

- 1) Each edge $e \in \pi$ has at least one pair available for swapping after optional purification (and storage decay when $T_{\text{mem}} > 1$);
- 2) All $k - 1$ BSMs on π succeed (probability q^{k-1});
- 3) The resulting end-to-end fidelity satisfies $F_{\text{end}}(\pi) \geq F_{\min}$.

Let $Y_t^{(s,d)} \in \{0, 1\}$ be the indicator of this event. If multiple edge-disjoint paths are activated in the same slot, we attempt them independently; independence across edge-disjoint paths follows from Remark 1 and disjoint resource usage. The per-slot throughput is $N_{\text{succ}}(t) = \sum_{(s,d) \in \mathcal{P}} Y_t^{(s,d)}$.

Although path feasibility is described in terms of the simple support graph \mathcal{H}_t , simultaneous path activations are constrained by the retained-pair multiplicities $N_t^{\text{ret}}(e)$. Each stored entangled pair can be consumed by at most one swapping operation in a slot. Consequently, if two candidate paths (possibly serving different source–destination pairs) share an edge

e , they may be activated in the same slot only if $N_t^{\text{ret}}(e) \geq 2$; when $N_t^{\text{ret}}(e) = 1$, at most one such path can be scheduled. This exclusivity is enforced by the controller action $a(t)$.

E. Controller Actions and Constraints

At each slot t , the controller observes the realized external successes $\{N_t^{\text{ret}}(e)\}$ defining $\mathcal{H}_t^{\text{multi}}$ and the fidelity–age states of all stored pairs. It then selects an action

$$a(t) \in \mathcal{A}_t = \{\text{choose up to } R \text{ flow-path activations and optional purifications}\},$$

subject to the following constraints:

- Attempt budget: at most R activations per slot;
- Local exclusivity: each stored pair is used at most once; purification consumes two pairs on the same link;
- Memory: a node stores at most $m_{\max}(e)$ pairs per edge, each expiring after T_{mem} slots under the decoherence law (2).

No cross-slot coordination or global optimization is assumed; the resulting dynamics are Markovian.

F. Homogeneous and heterogeneous regimes

Let a simple path $\pi = (e_1, \dots, e_k)$ comprise k edges. Under homogeneous assumptions

$$S(e) \equiv S, \quad p_0(e) \equiv p_0, \quad q \text{ constant}, \quad F_0(e) \equiv F_0,$$

each edge succeeds independently with probability

$$p_{\text{link}} = 1 - (1 - p_0)^S.$$

Hence, by independence,

$$\Pr\{\pi \subseteq \mathcal{H}_t\} = \prod_{j=1}^k \Pr\{e_j \in \mathcal{H}_t\} = (p_{\text{link}})^k.$$

Conditional on this event, the $k-1$ intermediate BSMs succeed independently with probability q^{k-1} . Therefore, the unconditional probability that path π yields one end-to-end ebit in slot t is

$$P_{\text{e2e}}(\pi) = (p_{\text{link}})^k q^{k-1}.$$

Numerical results also consider heterogeneous links with $L(e)$ drawn from an interval, leading to edge-dependent $p_0(e)$ and baseline fidelities $F_0(e)$ (via hardware- or distance-dependent calibration). In all heterogeneous experiments we keep (3) for fidelity composition and (2) for storage decay.

Remark 2 (Stationarity). Under Remark 1 and fixed parameters, the external multigraph process $\{\mathcal{H}_t^{\text{multi}}\}$ is i.i.d. across slots; with $T_{\text{mem}} > 1$ the joint state (stored-pair inventories with ages) is a time-homogeneous Markov chain. These properties are the basis for renewal and steady-state analyses used later.

IV. Problem Statement

This section formalizes the Fidelity-Age (FA) control problem by defining the usable-delivery process, the resulting FA dynamics, and the optimization objective under the system constraints introduced in Sec. III.

A. Usable-delivery process

From Sec. III, in each slot t the controller observes the random multigraph $\mathcal{H}_t^{\text{multi}}$ of link-level successes and executes internal operations according to its chosen action $a(t)$. Let $Y_t^{(s,d)} \in \{0, 1\}$ denote the event that request $(s, d) \in \mathcal{P}$ receives a usable entangled pair in slot t , i.e.,

$$Y_t^{(s,d)} = \mathbf{1}\{\exists \pi \subseteq \mathcal{H}_t \text{ selected by } a(t) : \pi \text{ connects } (s, d), \text{ all swaps succeed, and } F_{\text{end}}(\pi) \geq F_{\text{min}}\}.$$

The selection by $a(t)$ ensures that no physical entangled pair is used by more than one path in the same slot. Usable deliveries depend on the realized external successes, any applied purifications, storage decay, and the controller's scheduling choice.

B. Fidelity-Age (FA)

For each request (s, d) define the sequence of usable-delivery epochs

$$t_1^{(s,d)} < t_2^{(s,d)} < \dots, \quad t_{n+1}^{(s,d)} = \inf\{t > t_n^{(s,d)} : Y_t^{(s,d)} = 1\}.$$

The Fidelity-Age process measures the number of slots since the most recent usable delivery,

$$A_{s,d}(t) = t - \max\{t_n^{(s,d)} \leq t\}, \quad (4)$$

with $A_{s,d}(t) = t$ if no usable delivery has yet occurred. $A_{s,d}(t)$ increases linearly between deliveries and resets to 0 whenever $Y_t^{(s,d)} = 1$.

C. Optimization objective

Controller decisions obey the per-slot constraints defined in Sec. III-E. The performance metric of interest is the long-run time-average Fidelity-Age,

$$\bar{A}_{s,d} = \limsup_{n \rightarrow \infty} \frac{1}{n} \sum_{t=1}^n A_{s,d}(t), \quad (5)$$

and the system objective is to minimize a weighted sum of these averages:

$$\min_{\phi \in \Phi} \sum_{(s,d) \in \mathcal{P}} w_{s,d} \bar{A}_{s,d}, \quad \text{s.t. feasibility and budget constraints,} \quad (6)$$

where Φ is the set of stationary nonanticipative control policies and $\{w_{s,d}\}$ are fixed nonnegative weights.

D. Slot-level success probability

For a path $\pi = (e_1, \dots, e_k)$ activated in slot t , the unconditional probability of a usable delivery is

$$P_{\text{use}}(\pi) = \left(\prod_{j=1}^k p_{\text{link}}(e_j) \right) q^{k-1} \mathbf{1}\{F_{\text{end}}(\pi) \geq F_{\min}\}. \quad (7)$$

In the homogeneous regime, $p_{\text{link}}(e) \equiv p_{\text{link}}$ and $P_{\text{use}}(\pi) = p_{\text{link}}^k q^{k-1}$ whenever $F_{\text{end}}(\pi) \geq F_{\min}$.

E. Renewal interpretation

Under Remark 1 and any stationary policy $\phi \in \Phi$, the joint process $\{Z_t\}$ of system states is a time-homogeneous Markov chain. If for every (s, d) the inter-delivery time $\tau^{(s,d)} = t_{n+1}^{(s,d)} - t_n^{(s,d)}$ has finite second moment, then standard renewal theory yields

$$\bar{A}_{s,d} = \frac{\mathbb{E}[(\tau^{(s,d)})^2]}{2 \mathbb{E}[\tau^{(s,d)}]}. \quad (8)$$

This identity connects slot-level success probabilities in (7) to long-run FA performance and underlies the policy analysis in Sec. V.

V. Analysis

We analyze the Fidelity-Age (FA) process under a stationary control policy ϕ using renewal theory on the slotted quantum-network model.

A. Renewal formulation

Let Y_t denote the single-flow usable-slot indicator from Sec. IV-A (we drop (s, d) for brevity).

Let the inter-delivery interval be

$$\tau = \inf\{\ell \geq 1 : Y_{t+\ell} = 1 \mid Y_t = 1\}, \quad (9)$$

measured in slots of duration Δ . The renewal epochs $\{t_k\}$ correspond to times when a usable Bell pair is delivered.

Theorem 1 (FA renewal identity). Fix a slot duration $\Delta > 0$ and a stationary policy ϕ . Let $Y_t \in \{0, 1\}$ be the usable-delivery indicator from Sec. IV-A and let $\tau = \inf\{\ell \geq 1 : Y_{t+\ell} = 1\}$.

$1 \mid Y_t = 1\}$ be the inter-delivery time (in slots). Assume the underlying state process

$$Z_t = (\mathcal{H}_t^{\text{multi}}, \text{stored-pair inventories and ages, } a(t))$$

is stationary and ergodic under ϕ , that $0 < \Pr\{Y_t = 1\} < 1$, and that $\mathbb{E}[\tau] < \infty$ and $\mathbb{E}[\tau^2] < \infty$. Then the long-run average Fidelity–Age for flow (s, d) exists and

$$\bar{A}_{s,d} = \frac{\mathbb{E}[(\Delta\tau)^2]}{2\mathbb{E}[\Delta\tau]} = \Delta \frac{\mathbb{E}[\tau^2]}{2\mathbb{E}[\tau]}. \quad (10)$$

Proof sketch. Let $\{\sigma_n\}$ be delivery epochs (in continuous time) with inter-delivery lengths τ_n (in slots), i.e., $\sigma_{n+1} - \sigma_n = \Delta\tau_n$. Between σ_n and σ_{n+1} the age grows linearly from 0 to $\Delta\tau_n$ (continuous evolution within slots). The cycle reward is the time–integral of age,

$$R_n = \int_{\sigma_n}^{\sigma_{n+1}} A_{s,d}(u) du = \frac{1}{2}(\Delta\tau_n)^2 = \frac{\Delta^2}{2} \tau_n^2.$$

By the renewal–reward theorem, under the stated assumptions,

$$\bar{A}_{s,d} = \lim_{t \rightarrow \infty} \frac{\sum_{n: \sigma_n < t} R_n}{t} = \frac{\mathbb{E}[R]}{\mathbb{E}[\Delta\tau]} = \Delta \frac{\mathbb{E}[\tau^2]}{2\mathbb{E}[\tau]},$$

which yields (10). \square

B. Closed-form geometric case

If the usable-slot success probability is constant, $p_{\text{succ}} = \Pr\{Y_t = 1\}$, then $\tau \sim \text{Geom}(p_{\text{succ}})$, and

$$\bar{A}_{s,d} = \frac{\Delta}{2} \frac{2-p_{\text{succ}}}{p_{\text{succ}}}. \quad (11)$$

This expression defines the FA–success trade-off and is used for simulation baseline validation. The derivative $\partial\bar{A}_{s,d}/\partial p_{\text{succ}} = -\Delta/(2p_{\text{succ}}^2)$ confirms that FA decreases monotonically with p_{succ} but with diminishing benefit as $p_{\text{succ}} \rightarrow 1$.

C. Slot-level success probability

Consider homogeneous links with per-slot external success p_{link} and swap reliability q . A path π of k edges is usable with probability

$$P_{\text{use}}(\pi) = p_{\text{link}}^k q^{k-1} \mathbf{1}\{F_{\text{end}}(\pi) \geq F_{\min}\}. \quad (12)$$

If one purification round precedes each swap, with success map $P_{\text{pur}}(F_1, F_2)$ and output fidelities F'_ℓ , then

$$\begin{aligned} P_{\text{use}}(\pi) &= \mathbb{E}[\mathbf{1}\{\pi \subseteq \mathcal{H}_t\} \prod_{\ell \in \pi} P_{\text{pur}}(F_{1,\ell}, F_{2,\ell}) q^{k-1} \\ &\quad \mathbf{1}\{F_{\text{end}}(\{F'_\ell\}) \geq F_{\min}\}]. \end{aligned} \quad (13)$$

When κ paths π_1, \dots, π_κ are activated such that no physical entangled pair is shared across paths (i.e., they are disjoint in the multigraph $\mathcal{H}_t^{\text{multi}}$), independence implies

$$p_{\text{succ}} = 1 - \prod_{i=1}^{\kappa} (1 - P_{\text{use}}(\pi_i)) \approx \sum_{i=1}^{\kappa} P_{\text{use}}(\pi_i)$$

for small $P_{\text{use}}(\pi_i)$, showing that parallelism improves the slot-level success probability in the low-success regime.

D. Finite-FA conditions and stability

Finite $\bar{A}_{s,d}$ requires $\mathbb{E}[\tau^2] < \infty$. This holds whenever per-link and per-swap success probabilities are bounded below by $p_- > 0$ and $q_- > 0$, and the policy attempts at least one finite-length path with positive probability. Then τ is stochastically dominated by a geometric variable, ensuring $\bar{A}_{s,d} < \infty$. These conditions cover all simulation settings in Section VI.

E. Control sensitivity and scheduling

Combining (10)–(13), any action that increases the conditional success probability $\Pr\{Y_t = 1 \mid \text{state at } t, a(t)\}$ reduces FA. Hence, the controller should maximize the expected slot-level success given the observed state:

$$a^*(t) = \arg \max_{a \in \mathcal{A}_t} \mathbb{E}[Y_t \mid \text{state at } t, a], \quad (14)$$

subject to the per-slot attempt and memory limits. Equation (14) represents a drift-minimizing heuristic analogous to Lyapunov optimization in queueing networks and motivates the FA-THR and FA-INDEX schedulers analyzed later.

VI. Numerical Results

Monte Carlo simulations were carried out using the probabilistic slotted model described in Section III. Each experiment covers 2×10^5 slots with a 2×10^4 -slot warm-up and five random seeds. The network is a 3×3 grid supporting $|P|=16$ source–destination pairs with an attempt budget $R=8$ per slot ($R/|P|=0.5$). Unless otherwise stated, parameters are $\alpha=0.046 \text{ km}^{-1}$, $S=8$, BSM success $q=0.95$, $F_{\text{base}}=0.82$, and $F_{\text{min}}=0.75$.

A. Algorithms and Benchmarks

We evaluate four schedulers: two conventional baselines and two FA-aware designs. At each slot t , a controller selects a subset $\mathcal{S}_t \subseteq \mathcal{P}$ of flows to serve, under the per-slot budget $|\mathcal{S}_t| \leq R$.

Conventional baselines. TP-MAX chooses \mathcal{S}_t maximizing expected successful entanglements $\sum_{(s,d) \in \mathcal{S}_t} \hat{p}_{sd}(t)$, where $\hat{p}_{sd}(t)$ is the estimated success probability. FID-MAX replaces $\hat{p}_{sd}(t)$ with the expected end-to-end fidelity $\hat{F}_{sd}(t)$. Both greedily optimize instantaneous utility and ignore flow-age evolution.

FA-aware schedulers. Flow-age-aware control incorporates the penalty $A_{sd}(t)$ into the Lyapunov-drift rule

$$\mathcal{S}_t^* = \arg \max_{\mathcal{S} \subseteq \mathcal{P}, |\mathcal{S}| \leq R} \sum_{(s,d) \in \mathcal{S}} [U_{sd}(t) - \gamma A_{sd}(t)], \quad (15)$$

where $U_{sd}(t)$ is instantaneous utility and $\gamma > 0$ a sensitivity weight. We implement two low-complexity approximations:

FA-THR(τ) activates flows with $A_{sd}(t) > \tau$ and serves the R with highest $U_{sd}(t)$. Small τ favors throughput (TP-MAX limit), large τ promotes fairness.

FA-INDEX ranks flows by

$$I_{sd}(t) = U_{sd}(t) / (1 + \beta A_{sd}(t)), \quad (16)$$

serving the R largest indices. The parameter $\beta > 0$ controls the age-throughput trade-off; $\beta \rightarrow 0$ yields TP-MAX, and large β approaches equal-age service. Values $\beta \in [0.05, 0.2]$ are empirically stable.

Complexity. All schedulers require sorting at most $|\mathcal{P}|$ entries per slot: $\mathcal{O}(|\mathcal{P}| \log |\mathcal{P}|)$. FA-THR adds one comparison, and FA-INDEX adds a scalar weight, negligible for $|\mathcal{P}| \leq 16$. No global optimization or iterative search is needed.

Interpretation. Both FA-THR and FA-INDEX operationalize (15) by weighting utility with age. FA-THR provides a coarse serve/delay decision, while FA-INDEX yields smooth prioritization. Together they span the fairness-efficiency envelope of the Lyapunov-optimal policy.

B. Performance Metrics

Each simulation produces per-flow age traces $A_{sd}(t)$, the number of slots since the last usable entanglement for pair (s, d) . From these traces we compute the following metrics.

Mean Age.

$$\bar{A}_{sd} = \frac{1}{T} \sum_{t=1}^T A_{sd}(t), \quad \bar{A} = \frac{1}{|\mathcal{P}|} \sum_{(s,d) \in \mathcal{P}} \bar{A}_{sd}. \quad (17)$$

Tail Age (A_{95}).

$$A_{95} = \inf\{a : \Pr[A_{sd}(t) \leq a] \geq 0.95\}. \quad (18)$$

Extreme-Age Risk (CVaR₉₅).

$$\text{CVaR}_{95} = \mathbb{E}[A_{sd}(t) \mid A_{sd}(t) > A_{95}]. \quad (19)$$

Throughput.

$$\text{Thr} = \frac{1}{T} \sum_{t=1}^T N_{\text{succ}}(t), \quad (20)$$

where $N_{\text{succ}}(t)$ counts usable deliveries with $F_{sd}(t) \geq F_{\min}$.

Fairness. Jain's index on inverse ages serves as a service-rate proxy:

$$J = \frac{\left(\sum_{(s,d)} (1 + \bar{A}_{sd})^{-1} \right)^2}{|\mathcal{P}| \sum_{(s,d)} (1 + \bar{A}_{sd})^{-2}}. \quad (21)$$

Starvation.

$$S = \frac{1}{|\mathcal{P}|} \sum_{(s,d)} \mathbf{1}\{\bar{A}_{sd} > A_{\text{ref}}\}, \quad (22)$$

where A_{ref} is the 95th-percentile age of a single-flow baseline.

All metrics include 95% confidence intervals from batch-mean estimates across Monte-Carlo seeds and are referenced in Figs. 1a–1b and Table I.

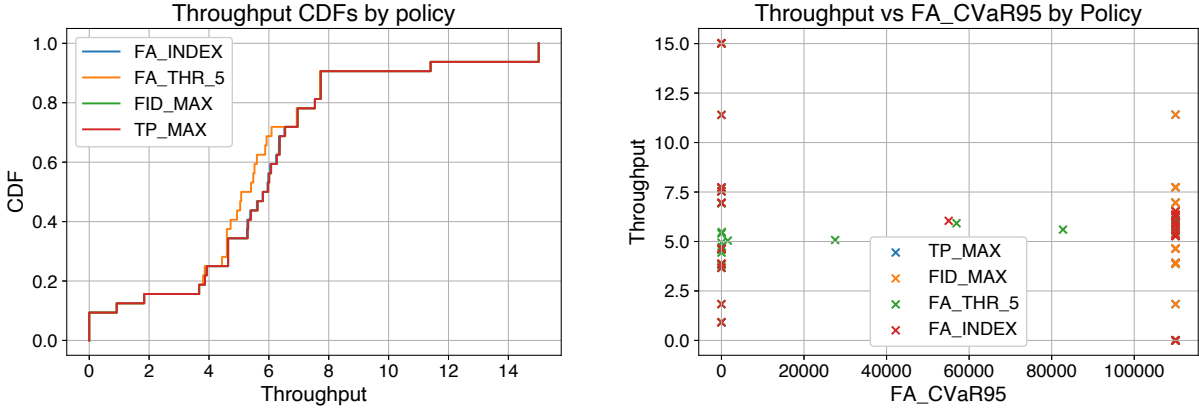
C. Baseline Validation

A single-flow configuration ($|\mathcal{P}|=1$, $R=1$) yields a mean flow age $\bar{A}=0.09$ and throughput $s \approx 0.918$ deliveries per slot. The close match between the simulated \bar{A} and the geometric prediction $\frac{1}{2} \frac{2-s}{s}$ validates both the stochastic event scheduler and the renewal approximation that underpins our analytical derivations. This agreement confirms that deviations observed in the multi-user setting stem from scheduling dynamics rather than model artifacts.

D. Load and Contention Effects

When multiple flows contend for limited transmission attempts, TP-MAX and FID-MAX greedily maximize instantaneous utility (throughput or fidelity) at the expense of temporal balance. This myopic prioritization allows a small subset of flows to monopolize resources, while others remain idle for extended periods. The outcome is a heavy-tailed flow-age distribution and catastrophic latency growth ($\bar{A} \approx 2.75 \times 10^4$, $A_{95} \approx 5.5 \times 10^4$) with roughly 25% starvation, as shown in Table I.

FA-aware schedulers, in contrast, internalize this temporal imbalance by explicitly penalizing aged flows. They occasionally defer high-utility transmissions to rejuvenate stale flows, thereby keeping the system near a quasi-stationary equilibrium. This adaptive balancing substantially improves fairness and stability: the cumulative distributions in Fig. 1a show



(a) CDF of per-flow ages $A_{sd}(t)$ showing the empirical distribution of flow-age samples used in Eqs. (17)–(19). FA-aware schedulers (FA-THR, FA-INDEX) exhibit sharply bounded tails, whereas throughput-driven baselines (TP-MAX, FID-MAX) produce heavy-tailed delay and starvation.

(b) Scatter plot of mean throughput (Eq. (17)) versus the 95% conditional value-at-risk of flow age (CVaR₉₅, Eq. (19)). Each point corresponds to one scheduler. FA-aware policies achieve Pareto-efficient trade-offs, maintaining throughput comparable to TP-MAX while reducing extreme-age risk by two orders of magnitude.

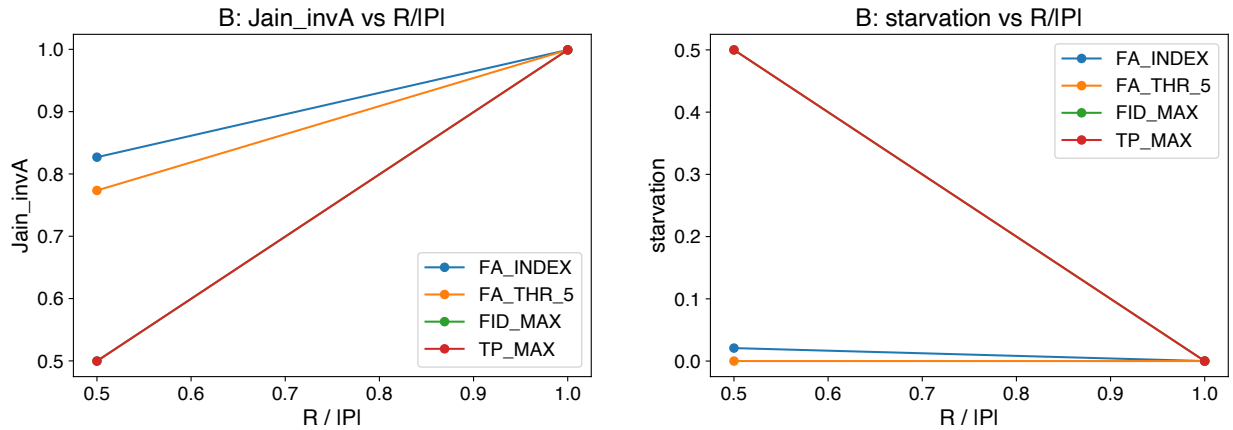
Fig. 1: 3×3 grid topology, $|P|=16$ source–destination pairs, attempt budget $R=8$ per slot ($R/|P|=0.5$), $q=0.95$, $F_{\min}=0.75$, no purification. Comparison of flow-age distributions and throughput–tail-age frontiers across scheduling policies.

that FA-aware policies dominate the tail region, eliminating the extreme delays characteristic of throughput-driven baselines. The resulting network state exhibits near-equalized service across flows, reflected in Jain’s index $J \approx 0.91$ and negligible starvation for FA-INDEX.

Figure 1b presents the throughput–tail-age frontier, comparing throughput against the 95% conditional value-at-risk (CVaR) of flow age. The behavior of FA-aware schedulers can be interpreted as a heuristic alignment with the control rule in (14). Since the long-run mean flow age \bar{A}_{sd} decreases monotonically with the usable-slot success probability s , Eq. (14) prescribes allocating transmission attempts to actions that most increase $\mathbb{E}[s(a(t))]$ per slot. FA-INDEX and FA-THR operationalize this idea by weighting each flow’s instantaneous utility by a decreasing function of its current age, effectively biasing service toward links whose success would yield the largest marginal reduction in expected age. Although these policies do not explicitly minimize a Lyapunov drift, their decisions empirically follow the same stabilizing direction, keeping the network near a balanced operating point with bounded flow ages.

TABLE I: Load contention on 3×3 grid ($|P|=16$, $R/|P|=0.5$, $F_{\min}=0.75$, no purification).

Policy	\bar{A}	A_{95}	Throughput	Jain	Starv.
TP-MAX	2.75×10^4	5.5×10^4	6.61	0.75	0.25
FID-MAX	2.75×10^4	5.5×10^4	6.61	0.75	0.25
FA-THR(5)	0.77	1.34	6.60	0.89	0.00
FA-INDEX	0.67	2.11	6.61	0.91	0.01



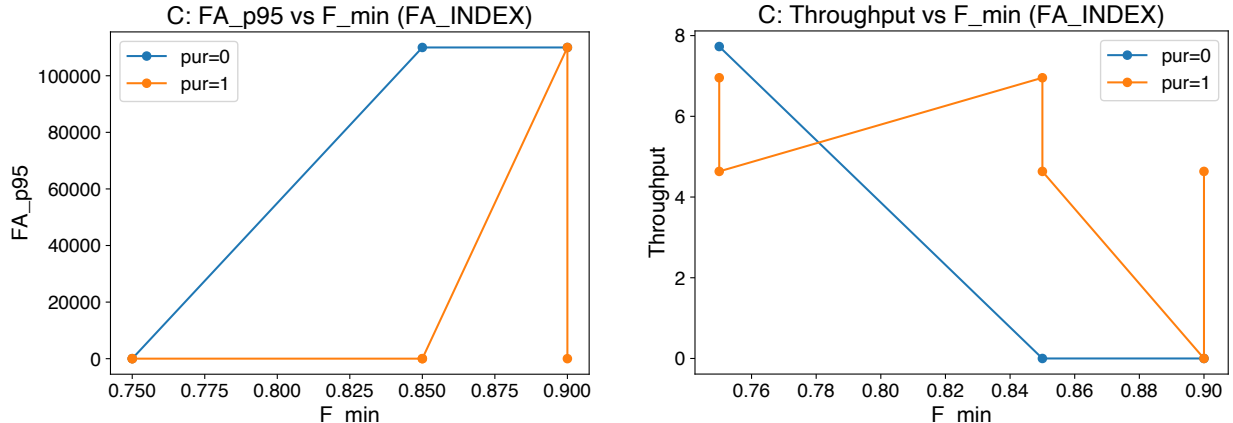
(a) Fairness measured by Jain's index J (Eq. (21)) computed on inverse mean ages $1/(1 + \bar{A}_{sd})$. FA-aware policies (FA-THR, FA-INDEX) sustain high fairness as the offered load $R/|P|$ increases, whereas throughput-oriented baselines collapse under contention.

(b) Starvation probability S (Eq. (22)) versus offered-load ratio $R/|P|$, where a flow is deemed starved if its mean age exceeds the single-flow 95th-percentile baseline A_{ref} . FA-aware scheduling nearly eliminates starvation even under half-budget load, evidencing strong temporal balancing across flows.

Fig. 2: 3×3 grid topology with $|P|=16$ flows and attempt-budget ratios $R/|P| \in \{0.5, 1.0\}$; $q=0.95$, $F_{\min}=0.75$, no purification. Comparison of fairness and starvation behavior across scheduling policies under varying network load.

E. Fidelity Constraints and Purification

Introducing purification and higher fidelity thresholds changes the trade-off surface between physical reliability and temporal freshness. As F_{\min} increases, usable entanglement success probability declines, reducing the effective service rate. Greedy policies amplify this effect because they repeatedly pursue high-fidelity paths that often fail, increasing age variance. In contrast, FA-aware schedulers naturally adapt: when the fidelity constraint makes a link unreliable, its age term grows, prompting reallocation toward shorter or more probable paths. Figures 3a–3b reveal that FA-INDEX and FA-THR maintain bounded flow ages



(a) 95th-percentile flow age A_{95} (Eq. (18)) versus minimum usable-fidelity threshold F_{\min} for the FA-INDEX scheduler. Increasing F_{\min} tightens the acceptance criterion and inflates A_{95} , reflecting longer waiting times for high-fidelity deliveries.

(b) Mean throughput Thr (Eq. (17)) versus F_{\min} . Purification improves achievable end-to-end fidelity but lowers the effective delivery rate, as more attempts fail to meet stricter thresholds.

Fig. 3: 3×3 grid, $|P|=8$, attempt-budget ratio $R/|P|=1$, BSM success $q=0.95$, purification success $p_{\text{pur}}=0.8$, and fidelity increment $\Delta F=0.08$. Comparison of latency and throughput effects as the fidelity threshold F_{\min} varies under FA-INDEX control.

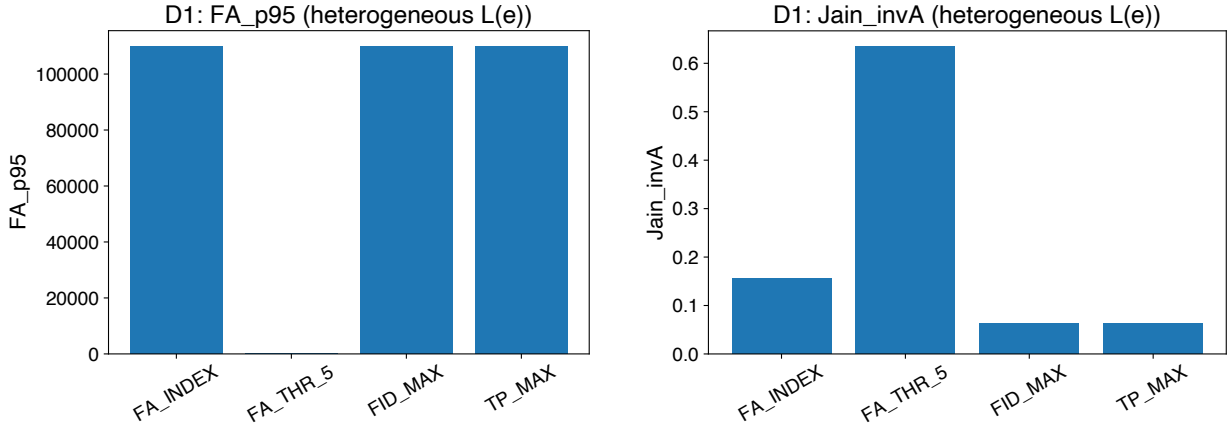
while throughput degrades smoothly. The slope of the FA_{95} curve reflects this adaptive balance—an indicator of resilience against physical-layer tightening.

F. Heterogeneous Path Lengths

Path-length heterogeneity introduces asymmetric success probabilities that challenge fairness mechanisms. Because FA-INDEX currently weighs all flows equally, its age term over-penalizes short paths and under-reacts to long, lossy ones. The outcome (Fig. 4a) is an inflated mean age for distant pairs and fairness loss ($J \approx 0.64$, Fig. 4b). FA-THR(5), which uses a simpler age-threshold trigger, performs better because it implicitly normalizes by success rate—flows with low link success accumulate age quickly and trigger service more often. These results highlight that FA-INDEX should incorporate per-path success expectations (e.g., p_e or end-to-end s_k) to remain optimal in heterogeneous networks.

G. Finite-Coherence Regime

As memory coherence degrades (smaller T_2 or larger waiting depth T), usable fidelities decay exponentially. This introduces time coupling: delayed deliveries not only increase age but also reduce future success probabilities. Greedy schedulers ignore this, causing cascading stalls



(a) 95th-percentile flow age A_{95} (Eq. (18)) per policy. FA-THR maintains bounded delay across heterogeneous routes, whereas FA-INDEX shows higher sensitivity to path length due to stronger age weighting.

(b) Fairness measured by Jain's index J (Eq. (21)) computed over inverse mean ages $1/(1 + \bar{A}_{sd})$. FA-THR provides the most uniform service across flows, while FA-INDEX slightly sacrifices fairness for lower tail age.

Fig. 4: 3×3 grid topology with random link lengths $L(e) \in [10, 80]$ km, producing path lengths $k \in \{2, 3, 4, 6\}$; $|P|=8$, $R/|P|=0.5$, BSM success $q=0.9$, no purification. Comparison of latency and fairness across policies under heterogeneous end-to-end distances.

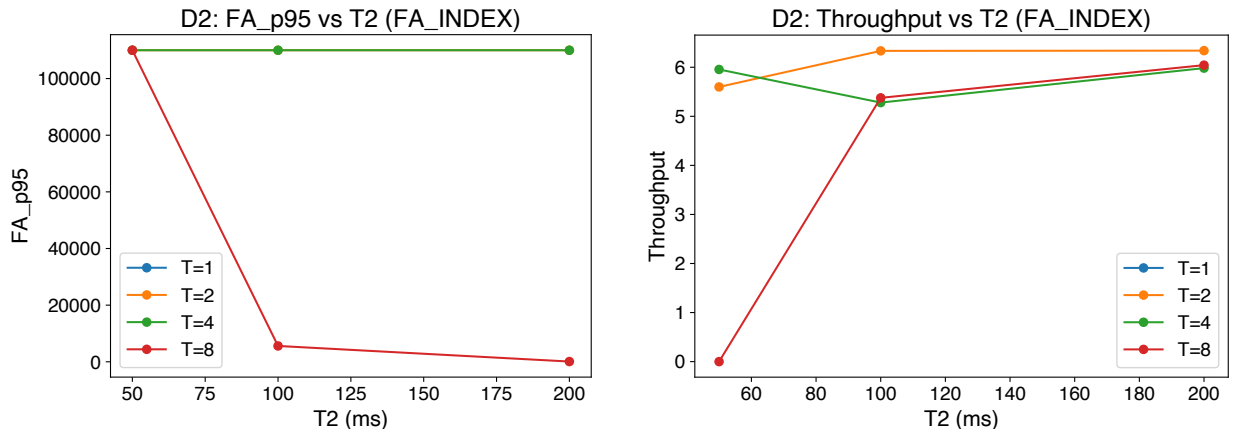
and rapidly increasing \bar{A} and A_{95} . FA-aware schedulers mitigate this feedback by accelerating service of older flows before fidelity loss becomes severe. Figure 5a shows that FA-THR maintains bounded ages even when coherence time drops below 100 ms, while FA-INDEX—tuned for memoryless links—degrades gradually. Throughput trends in Fig. 5b confirm that FA-awareness preserves operational efficiency by anticipating decoherence-induced service decay.

H. Pareto Frontier Analysis

The composite frontier in Fig. 6 summarizes the overall trade-off between efficiency (throughput) and temporal freshness (FA_{95}). Points corresponding to FA-THR and FA-INDEX dominate the Pareto boundary across all load regimes, whereas TP-MAX and FID-MAX cluster far from the efficient region. This demonstrates that enforcing temporal balance via flow-age control yields globally superior operating points—no policy can jointly improve both throughput and latency without incorporating some form of FA-awareness.

I. Discussion and Insights

The results show that flow-age weighting serves as a distributed regulator aligning short-term scheduling with long-term temporal stability. Purification and fidelity constraints interact



(a) 95th-percentile flow age A_{95} (Eq. (18)) versus coherence time T_2 for the FA-INDEX policy. Shorter coherence periods cause rapid latency inflation, especially on long paths, as stored qubits decohere before successful end-to-end completion.

(b) Mean throughput Thr (Eq. (17)) versus coherence time T_2 . All schedulers suffer rate loss from decoherence, but FA-aware control maintains higher throughput by refreshing stale links and prioritizing high-success paths within the coherence window.

Fig. 5: 3×3 grid topology, $|P|=8$, attempt-budget ratio $R/|P|=1$, BSM success $q=0.9$, no purification, memory delay $T \in \{2, 4, 8\}$ slots, and coherence times $T_2 \in \{50, 100, 200\}$ ms. Comparison of latency and throughput degradation under finite-memory effects for FA-INDEX and other schedulers.

multiplicatively with age, requiring joint adaptation of fidelity targets and age weights. In heterogeneous or decoherence-limited regimes, FA-INDEX should normalize by estimated success probabilities to preserve fairness. Overall, the FA-aware policies behave as dynamic backlog-balancing controllers that approximately minimize age drift, linking physical-layer reliability with network-layer fairness and establishing age-driven scheduling as a unifying principle for stable quantum networks.

VII. Conclusions

We introduced the Fidelity-Age (FA) metric as a joint measure of timeliness and fidelity for quantum repeater networks, capturing the time elapsed since the most recent delivery whose end-to-end fidelity exceeds a prescribed threshold. By modeling usable entanglement deliveries as renewal events, we established an explicit analytical relationship between slot-level success probabilities and long-run average FA, enabling principled performance evaluation under stochastic generation, swapping, and decoherence.

Formulating FA minimization under finite memory, attempt budgets, and fidelity con-

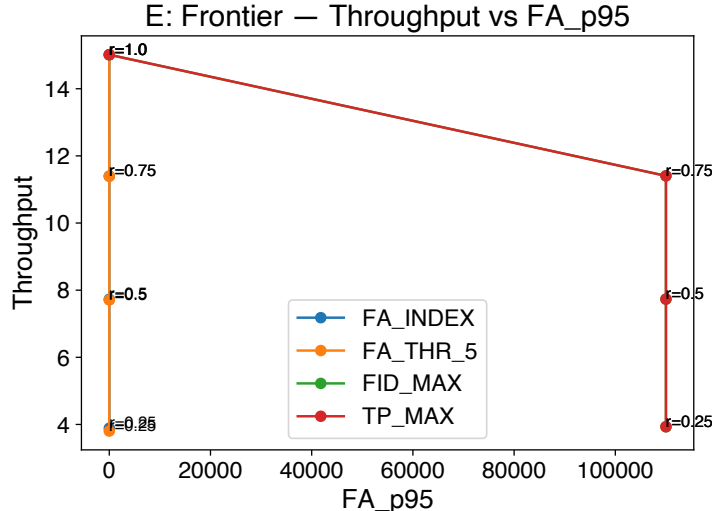


Fig. 6: Each point represents the mean throughput Thr (Eq. (17)) and the corresponding 95th-percentile flow age A_{95} (Eq. (18)) averaged over 20 Monte Carlo seeds. Pareto frontiers illustrate the trade-off between delivery rate and latency tail. FA-aware schedulers trace the Pareto-efficient frontier, maintaining high throughput with markedly smaller tail ages than throughput-driven baselines.

straints led to two lightweight scheduling policies, FA-THR and FA-INDEX, which approximate Lyapunov-drift-optimal control while remaining implementable with local state information. These policies directly target freshness-conditioned usability rather than instantaneous throughput alone.

Simulation results demonstrate that FA-aware scheduling preserves throughput while substantially improving fairness and stability, suppressing extreme-age tails even in heterogeneous networks with finite coherence times. More broadly, explicit age-based weighting provides a systematic mechanism for balancing short-term transmission opportunities against long-term delivery regularity, suggesting FA as a unifying objective for freshness-aware control in quantum networks.

References

- [1] H. J. Kimble, “The quantum internet,” *Nature*, vol. 453, pp. 1023–1030, 2008.
- [2] S. Wehner, D. Elkouss, and R. Hanson, “Quantum internet: A vision for the road ahead,” *Science*, vol. 362, no. 6412, 2018.
- [3] H.-J. Briegel, W. Dür, J. I. Cirac, and P. Zoller, “Quantum repeaters: The role of imperfect local operations in quantum communication,” *Phys. Rev. Lett.*, vol. 81, no. 26, p. 5932, 1998.
- [4] W. Dür, H.-J. Briegel, J. I. Cirac, and P. Zoller, “Quantum repeaters based on entanglement purification,”

Phys. Rev. A, vol. 59, no. 1, p. 169, 1999.

[5] M. Pant, H. Krovi, D. Towsley, L. Tassiulas, and L. Jiang, “Routing entanglement in the quantum internet,” npj Quantum Information, vol. 5, no. 25, 2019.

[6] N. H. Nickerson, J. F. Fitzsimons, and S. C. Benjamin, “Freely scalable quantum technologies using cells of 5-to-50 qubits with very lossy and noisy photonic links,” Phys. Rev. X, vol. 4, no. 4, p. 041041, 2014.

[7] S. E. Vinay and P. Kok, “Practical repeaters for ultralong-distance quantum communication,” Phys. Rev. A, vol. 95, p. 052336, May 2017. [Online]. Available: <https://link.aps.org/doi/10.1103/PhysRevA.95.052336>

[8] K. Azuma, N. Sota, M. Koashi, and N. Imoto, “Tight bound on coherent-state-based entanglement generation over lossy channels,” Phys. Rev. A, vol. 81, p. 022325, Feb 2010. [Online]. Available: <https://link.aps.org/doi/10.1103/PhysRevA.81.022325>

[9] R. Van Meter et al., “Path selection for quantum networks,” Netw. Sci., vol. 3, pp. 82–95, 2013.

[10] S. Kaul, R. D. Yates, and M. Gruteser, “Real-time status: How often should one update?” in Proc. IEEE INFOCOM, 2012, pp. 2731–2735.

[11] I. Kadota, A. Saha, and E. Modiano, “Scheduling algorithms for optimizing age of information in wireless networks,” IEEE/ACM Transactions on Networking, vol. 27, no. 6, pp. 2543–2556, 2019.

[12] K. Azuma, S. Takeda, K. Kato et al., “Quantum repeaters: From quantum networks to the quantum internet,” Reviews of Modern Physics, vol. 95, p. 045006, 2023.

[13] Y. Lee, E. Bersin, A. Dahlberg, S. Wehner, and D. Englund, “A quantum router architecture for high-fidelity entanglement flows in quantum networks,” npj Quantum Information, vol. 8, p. 75, 2022.

[14] J. Halder, A. Rajabov, R. Bassoli, F. H. P. Fitzek, and G. P. Fettweis, “Optimal routing and end-to-end entanglement distribution in quantum networks,” Scientific Reports, vol. 14, p. 19262, 2024.

[15] A. Patil et al., “Entanglement generation in a quantum network at distance-independent rate,” npj Quantum Information, vol. 8, p. 180, 2022.

[16] S. DiAdamo and J. N’otzel, “Packet switching in quantum networks: A path to the quantum internet,” Physical Review Research, vol. 4, p. 043064, 2022.

[17] Z. Xiao, J. Li, K. Xue, N. Yu, R. Li, Q. Sun, and J. Lu, “Purification scheduling control for throughput maximization in quantum networks,” Communications Physics, vol. 7, no. 1, p. 307, 2024.

[18] V. Semenenko, X. Hu, E. Figueroa, and V. Perebeinos, “Entanglement generation in a quantum network with finite quantum memory lifetime,” AVS Quantum Science, vol. 4, no. 1, p. 012002, 2022.

[19] A. Fayyaz, P. Krishnamurthy, K. P. Seshadreesan, D. Tipper, and A. Babay, “On selecting paths for end-to-end entanglement creation in quantum networks,” 2025. [Online]. Available: <https://arxiv.org/abs/2505.02283>

[20] H. Gu, W. Liu, Y. Liu, J. Li, and Y. Luo, “Esdi: Entanglement scheduling and distribution in the quantum internet,” arXiv preprint arXiv:2303.17540, 2023.

[21] S. Bhambay and E. Modiano, “Optimal scheduling in a quantum switch,” arXiv preprint arXiv:2501.05380, 2025.

[22] G. Ni, L. Ho, and H. Claussen, “Entanglement request scheduling in quantum networks using deep q-network,” 2025. [Online]. Available: <https://arxiv.org/abs/2505.12461>

[23] M. A. Nielsen and I. L. Chuang, Quantum Computation and Quantum Information: 10th Anniversary Edition. Cambridge University Press, 2010.

[24] C. H. Bennett, G. Brassard, S. Popescu, B. Schumacher, J. A. Smolin, and W. K. Wootters, “Purification of noisy entanglement and faithful teleportation via noisy channels,” Phys. Rev. Lett., vol. 76, pp. 722–725, Jan 1996. [Online]. Available: <https://link.aps.org/doi/10.1103/PhysRevLett.76.722>